Microchimica Acta (2022) 189:382
https://doi.org/10.1007/s00604-022-05479-z

ORIGINAL PAPER

Screening of dopamine in living cells and animal model via graphene quantum dots anchored 3D macroporous nonenzymatic sensor

Kun Wang[1] · Yige Li[1] · Manlin Qi[1] · Chunyan Li[1] · Biao Dong[2] · Lin Xu[2] · Lin Wang[1]

Received: 6 July 2022 / Accepted: 26 August 2022 / Published online: 14 September 2022

Abstract

A series of three-dimensional copper oxide (CuO) inverse opals anchored with carboxylated graphene quantum dots (CuO/cGQDs) have been fabricated for non-enzymatic tracking of dopamine (DA). Heterostructures composed of various building blocks are promising to construct versatile biosensing platforms. The optimal CuO/cGQDs modified electrode demonstrates sensitivities of 243.45 μA mM^{-1} cm^{-2} (50 nM–1888.5 μM) with the practical detection limit as low as 0.5 nM in mimic physiological environment (at + 0.45 V vs. Ag/AgCl). The extraordinary tolerance to various interferents enables the practical detection of intracellular DA amount in human neural cells. On this basis, the proposed biosensor attains precise evaluation of antipsychotic drug effects on stimulated DA release. Particularly, it successfully spots fluctuation of DA in plasma and cerebrospinal fluid in murine model of Parkinson's disease, which serves as a crucial tool to understand neuropathology and symptomatology of DA-related diseases. This study developed a reliable sensing platform and is expected to be applied to physiological and pathological studies.

Keywords Electrochemical sensor · Amperometry · Inverse opal · Quantum dots · Dopamine · Live cells · Animal model

Introduction

Dopamine (DA) is a common catecholamine neurotransmitter of optimum significance for regulating physiological operation of central and peripheral nervous systems [1]. However, DA dysfunction is allied with occurrence of diverse neurological diseases like Parkinson's disease (PD), senile dementia, epilepsy, schizophrenia and euphoria, etc. [2]. Moreover, DA detection is greatly hampered by the ultralow concentration in biofluid along with interference from co-existed ascorbic acid (AA) and uric acid (UA) [3]. Therefore, the rapid and precise determination and tracking fluctuating level of DA is of significance and desirable in fundamental pathophysiological research as well as in biomedical diagnosis and therapeutics.

For decades, it has been deeply investigated to monitor DA concentration by numerous approaches such as luminescent approach, mass spectroscopy, and fluorescent strategy. However, these methods are expensive and they require complicated preparation, specialized equipment, and time-consuming analysis [4]. Nowadays, electrochemical techniques take prevalence on account of their unparalleled merits including low cost, high efficiency, time-saving fabrication, and long-term recognition, which suit the detection of neurotransmitters perfectly [5]. Specially, DA can take few efforts to electrochemically realize direct oxidation or reduction at low potentials owing to the redox-active property [6]. Currently, most electrochemical biosensors investigate the sensing feasibility by testing human serum spiked with DA or neural cells (secreted DA upon K^+ stimulation). Both methods are imperative to demonstrate brilliant DA monitoring capability even in complex and dynamic environment. However, the DA determination in real pathological samples for DA-related diseases is rarely implemented, thus lack of the direct evidence to learn about neurological processes of DA-related diseases in real complex pathological

✉ Biao Dong
dongb@jlu.edu.cn

✉ Lin Xu
linxu@jlu.edu.cn

✉ Lin Wang
wanglin1982@jlu.edu.cn

[1] Department of Oral Implantology, School and Hospital of Stomatology, Jilin University, Changchun 130021, China

[2] State Key Laboratory On Integrated Optoelectronics, Collage of Electronic Science and Engineering, Jilin University, Changchun 130021, China

environment. Recently, animal model of DA-related diseases is constructed as more intuitional tool to learn about symptomatology and neuropathology of PD from the behavioral state and biofluid sample [7, 8]. Nevertheless, more biosensors are still needed to investigate correlation between DA level fluctuations and specific behavioral activities in terms of real pathological model, which will definitely pave the way for recognition and long-term monitor of DA-related diseases.

In this regard, considerable amounts of efforts should be made to propose brilliant electrochemical monitoring strategies for determining DA in biofluids with time-saving manufacturing, excellent sensitivity, and good selectivity. Transition metal oxides (TMOs) are promising candidate in terms of stable structure, electrocatalytic nature, and extraordinary sensitivity [9]. Among these semiconductor materials, copper oxide (CuO), a simple p-type semiconductor, has been intensively investigated in DA determination owing to adequate catalytic active sites as well as good electrochemical redox capability. However, the poor electron shuttling capability and weak interaction between analyte and interface oppose great restrictions to the biological feasibility for electrochemical determination of CuO based DA sensor. In order to enhance the performance of CuO-based sensors, morphology modulation and heterostructure construction are two general approaches. Morphology modulation contributes to vast specific surface area along with higher interaction rate, while heterostructure construction works on enhancing the catalytic capabilities of the electrocatalyst [10]. As for morphology modulation, three-dimensional inverse opal (3DIO) suits perfectly to monitoring target analyte due to its high porosity, interconnected skeleton, and abundant active sites. However, when faced the complex background with trace DA concentration in biological environment, novel nanomaterial with extraordinary electroactive property and supreme affinity capability towards DA should be proposed.

As integrating the advantages of graphene and carbon quantum dots simultaneously, the superior conductivity of graphene quantum dots (GQDs) can greatly accelerate the electron transfer to facilitate the whole electrocatalytic process [11]. Moreover, beyond superior biocompatibility and stability of the GQDs compared with other QDs, such as PbS and CdS, the specific π–π stacking interactions between DA and graphene make it suitable candidate for DA sensing [12, 13]. Until now, Aoun's group has developed an electrochemical DA sensor modified by nitrogen-doped GQDs–chitosan (CS) nanocomposite, which attained excellent sensitivity of 418 μA mM^{-1} cm^{-2} [14]. Huang's group has constructed an ultrasensitive electrochemical DA sensor with modification of GQDs/multiwalled carbon nanotubes composite, possessing an ultralow detection limit of 0.87 Nm [15]. With addition of GQDs, all these biosensors attain good electrochemical monitoring capacity, originating from its fabulous affinity towards DA and high carrier mobility. Nonetheless, combination of GQDs and CuO has not been investigated for the electrochemical determination of DA in living cell or biofluid samples.

In this work, as shown in Scheme 1, carboxylated GQDs (cGQDs) were anchored onto 3DIO CuO to construct a brilliant electrochemical sensor for accurate and real-time detection of DA in artificial biofluid, stimulated neural cells and even real pathological sample from animal model. The 3DIO CuO was chosen for its electrochemical redox capability and abundant active sites in porous structure, which served as biomarker recognizing part. The cGQDs was selected for its good conductivity, biocompatibility, and high affinity towards DA (carboxyl-amino and π-π stacking interactions); these properties could well compensate the shortcomings of CuO in DA detection. What's important, the negatively charged (the zeta potential was approximately – 10.47 mV) CuO/cGQDs tended to interact with positively charged DA through electrostatic attraction, rather than negatively charged AA and UA which may cause negative repulsion. Together with the specific recognition of DA via carboxyl from cGQDs and amino from DA, the selectivity issues could be effectively enhanced. Due to superior biocompatibility, it successfully recognized fluctuation for DA efflux from PC12 cells upon K stimulation with and without pretreatment of antipsychotic drug (haloperidol). Ultimately, animal model of PD was constructed to investigate the feasibility for the biosensor to monitor DA fluctuation, which illustrated neurological processes of DA-related diseases in real complex pathological environment. The present study demonstrated promising potential for precise determination of DA for diagnosis and treatment on account of various DA-related neurological diseases.

Results and discussion

Characterization of CuO/cGQDs samples

The morphologies and microstructure of CuO/cGQDs were characterized by SEM and TEM measurements. As shown in Fig. 1A, the 3DIO CuO samples presented a long-range and well-ordered inverse opal structure, which was attributed to the ordered structure of the PMMA sphere templates (Fig. 1B) by self-assembly. Moreover, the average diameters (450 nm) of the original PMMA sphere templates were larger than the void opal size (300 nm) of the 3DIO CuO scaffold, which indicated size shrinkage owing to calcination. The TEM image in Fig. 1C showed the inheritance of the typical porous morphology of 3DIO CuO samples even after being scraped from the glass. Figure 1D showed that the cGQDs were uniform small round dots with a relatively limited size in range of 1–2 nm. The image of CuO/cGQDs

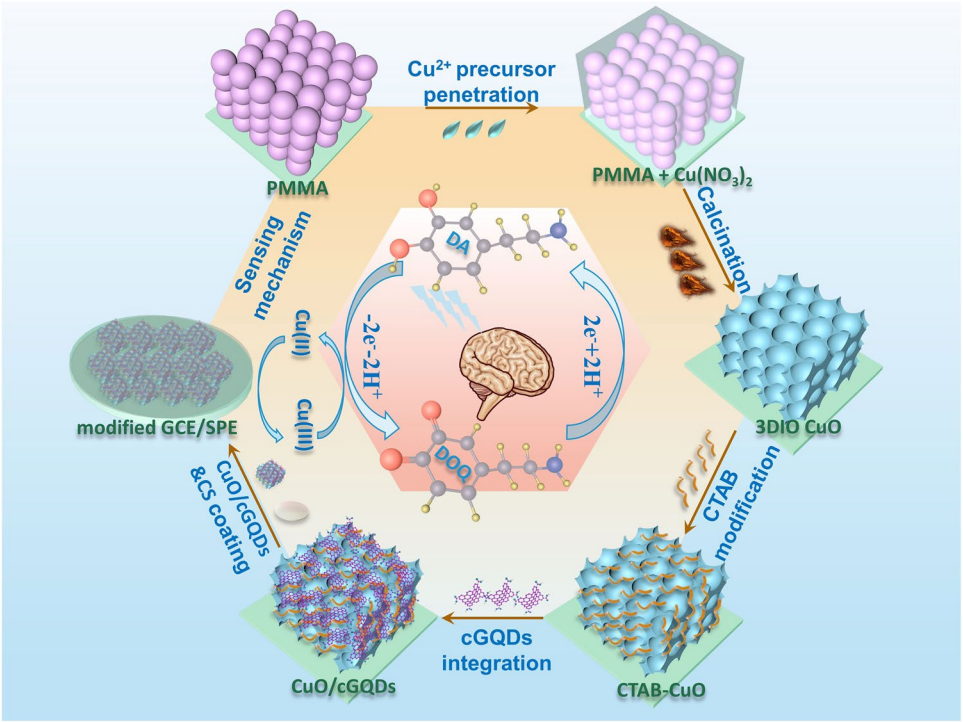

Scheme 1 Schematic image of synthesis and sensing mechanisms of the CuO/cGQDs nanocomposite. The Cu^{2+} precursor infiltrated PMMA templates was calcinated to attain 3DIO CuO, which was then modified by CTAB and integrated with cGQDs by mixing in solution sequentially. The detailed process for decoration of electrode: the CuO/cGQDs nanohybrid and CS were coated onto the GCE/SPE step by step. The electrooxidation mechanism: DA was oxidized to DOQ by Cu(III), who turned to Cu(II)

nanohybrid was displayed in Fig. 1E and the selected area was amplified for a clearer presentation (Fig. 1F) owing to the rather small size of cGQDs. Accordingly, the porous structure of CuO and tiny dot of cGQDs were simultaneously spotted, which confirmed the successful fabrication of the CuO/cGQDs heterostructure. Furthermore, for HRTEM image in Fig. 1G–H, lattice fringes of 0.232 nm (111) and 0.250 nm (002) respectively corresponded with the crystallographic planes of CuO and cGQDs. Both interplanar spacings could be observed in the Fig. 1I, which provided solid proof for the assembly of CuO and cGQDs. All above analysis indicated that cGQDs were homogeneously introduced onto the 3DIO CuO skeleton via electrostatic adsorption. Therefore, adequate surface area along with accelerated electron transfer process was achieved by such unique nanostructure, which in turn led to enhancement of electrocatalytic capability for sensitive electrochemical detection of DA.

Crystal phases of CuO/cGQDs composites were further examined by XRD patterns. As plotted in Fig. 2A, the (002) and (111) planes of cubic CuO (JCPDS#80-1917) were illustrated by two characteristic peaks situated at 35.2° and 38.3° respectively. As for cGQDs (JCPDS#04-0784), the typical refraction peak at 26.3° was well indexed to the (002) planes and the peak centered at 13.7° was assigned to the additional functional groups of carboxyl [16]. Notably, in the XRD patterns for CuO/cGQDs, distinct diffraction peaks for cGQDs were extremely weak due to extremely low diffraction intensity and little cGQDs ratio [17]. In short, the XRD results mentioned above further demonstrated the successful integration of target cGQDs and CuO.

Raman spectroscopy is an important technology for identification of graphene [18]. In Fig. 2B, the A_g and B_g vibration modes of CuO were manifested by the Raman peaks centered at 270, 318, and 615 cm^{-1}, which were simultaneously spotted in distinct spectrum of CuO and CuO/cGQDs nanohybrid [19]. Meanwhile, the peaks of D and G modes situated at 1392 and 1617 cm^{-1} were attributed to disordered sp^3 defects and the sp^2 C-C bond of carbon materials, which were spotted in the spectra of both cGQDs and CuO/cGQDs nanocomposite. However, the I_D/I_G ratio of CuO/cGQDs (1.02) was smaller than that of cGQDs (1.08), indicating the reduction of defects. This provided the target analyte with a smooth pathway and therefore enhanced catalytic activity of fabricated nanohybrids [20]. Moreover, compared with pristine CuO and cGQDs, the change in position and intensity of characteristic peaks demonstrated successful formation of heterostructure rather than a simple physical mixture of CuO and cGQDs.

The vibrational modes of as-prepared CuO/cGQDs composites were further investigated by the FTIR depicted in Fig. 2C. Considering CuO sample, the unique band (503 cm^{-1}) matched well with Cu-O elastic vibration [21]. To enhance adsorption capacity for cationic 3DIO CuO towards anionic cGQDs, CTAB (a cationic detergent) was introduced to provide cationic functional group for modification of 3DIO CuO [22]. As for CTAB, the deformation of $-CH_2-$ and $-CH_3$ groups was illustrated by the distinct

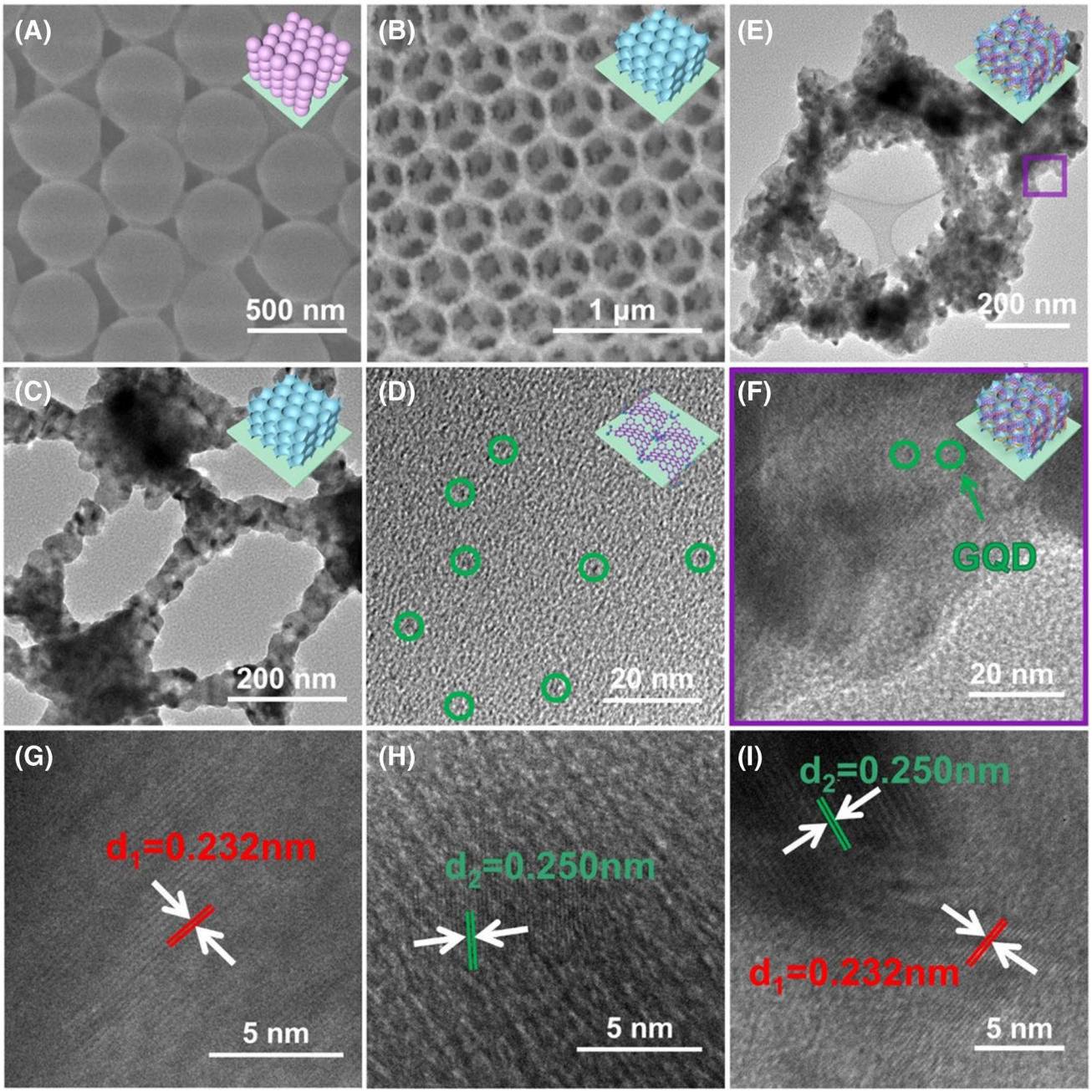

Fig. 1 Morphological characterization of CuO/cGQDs composites: (**A**, **B**) Typical SEM images of (**A**) PMMA and (**B**) 3DIO CuO; (**C**–**F**) TEM images and (**G**–**I**) corresponding HRTEM images of (**C**, **G**) CuO, (**D**, **H**) cGQDs, and (**E**, **F**, **I**) CuO/cGQDs nanocomposite. The selected area in (**E**) is magnified as (**F**)

bands centered at 1478 cm^{-1}; moreover, N-CH_3 symmetric stretching vibrations (2846 cm^{-1}) and C-CH_2 asymmetric stretching (2910 cm^{-1}) were spotted as well in the incorporated surfactants [23]. In the spectrum of cGQDs, the broad peak in spectrum of cGQDs at the range of 3200 to 3600 cm^{-1} revealed the presence of different OH groups. Vibration of C–O was manifested by distinct bands at around 1195 and 1397 cm^{-1}; meanwhile, stretching of the C = C and C = O bonds was demonstrated through the characteristic bands centered at 1562 and 1723 cm^{-1}, respectively [24]. In terms of CuO/cGQDs nanocomposite, characteristic bands for pristine CuO and cGQDs were presented in the spectrum, elucidating the successful assembly of such distinctive hybrid structure. Moreover, after the intergration of CuO and cGQDs, the shift for peak of C = O stretching vibration (1723 cm^{-1} to 1718 cm^{-1}) confirmed that the periphery

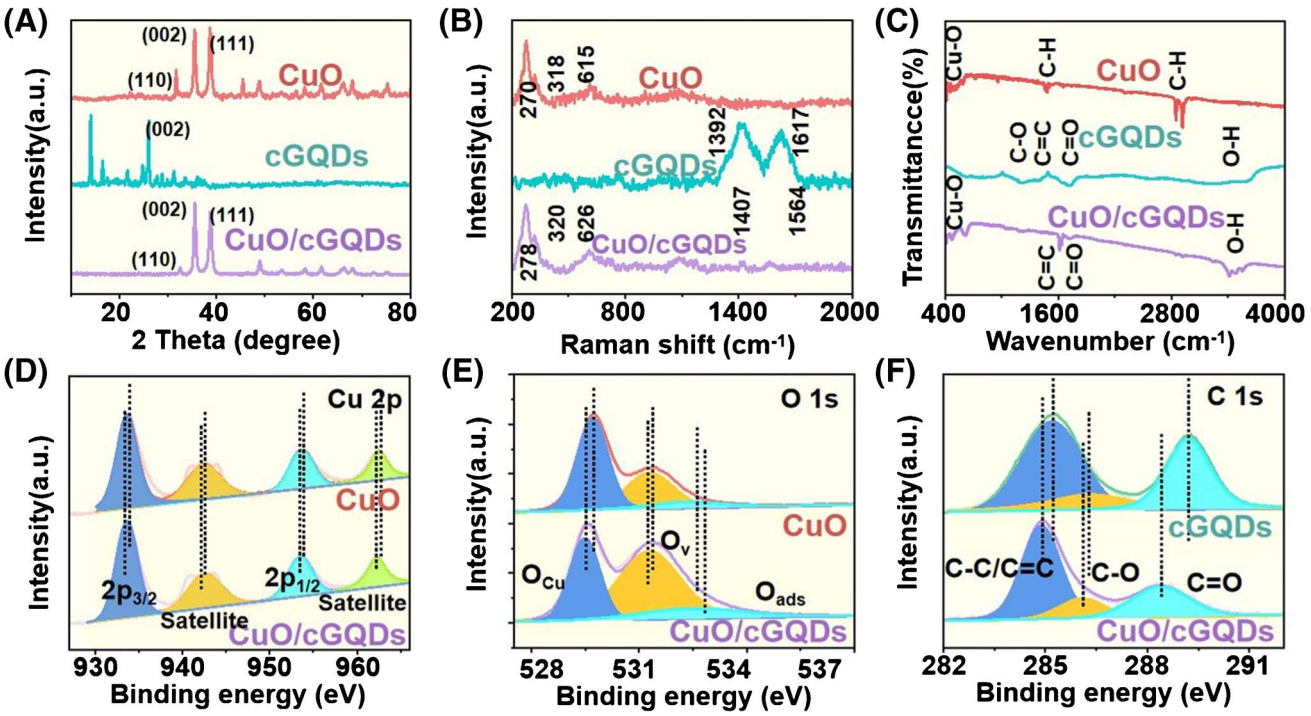

Fig. 2 Surface properties of CuO/cGQDs nanocomposite compared to those of pristine CuO and/or cGQD samples: (**A**) XRD patterns, (**B**) Raman spectrum, and (**C**) FTIR patterns of CuO, cGQDs and CuO/cGQDs. (**D**–**F**) High-resolution XPS spectra of (**D**) Cu 2p, (**E**) O 1 s, and (**F**) C 1 s

carboxylic groups of the cGQDs had been converted into carboxylate groups. This analysis demonstrated that the interfacial interaction of CuO and cGQDs was achieved via Cu-O bonds [25].

XPS analysis explores the valance state and composition for surface elements of the material. In Figure S1, Br 3d peak (78 eV), C 1 s peak (284 eV), O 1 s peak (533 eV), and Cu 2p peak (941 eV) were included in the whole XPS spectra of CuO/cGQDs composite, further confirming the co-existence of CTAB modified CuO and cGQDs. As Fig. 2D presented, the main peaks for Cu $2p_{3/2}$ (933.6 eV) and $Cu2p_{1/2}$ (953.7 eV) existed simultaneously in the characteristic Cu 2p spectrum of CuO and its nanohybrid. Furthermore, the typical shake-up satellite peaks appeared at the binding energy of 942.4 and 962.4 eV were assigned to Cu $2p_{3/2}$ and Cu $2p_{1/2}$, respectively. Compared with the pristine CuO, the characteristic Cu 2p peak shifted towards lower binding energy side in its nanohybrid, which was assigned to the interfacial interaction between CuO and cGQDs. According to previous literature, there were three components in the XPS spectrum of O 1 s (Fig. 2E): lattice oxygen (O_{Cu}), deficient oxygen (O_v), and adsorbed oxygen (O_{ads}) species, with corresponding peak centered at 529.7, 531.3, and 534.1 eV, respectively [26]. Due to diverse and complex chemical surrounding of O, binding energy and proportion of each distinct peak changed to some extent in the CuO/cGQDs composite. Especially the variation of corresponding O_v contents ($[O_v/(O_v + O_{Cu} + O_{ads})]$ area ratios), which were calculated to be 37.1% and 53.0% for CuO and CuO/cGQDs species, demonstrating that the fabricated nanocomposite obtained more surface oxygen vacancies [10]. In this way, electron mediator-oxygen vacancies were enhanced and the charge transfer was accelerated, contributing to improved electrocatalytic capability and brilliant electrochemical sensing performance [27]. Finally, Fig. 2F showed the C 1 s spectra of CuO/cGQDs nanohybrid along with the pristine cGQDs sample to verify the existence of diverse functional groups. Integration of sp^2 and sp^3 carbons (C = C and C–C) was manifested by the peak centered at 285.2 eV, attributing to the graphitic structure of cGQDs. Moreover, the deconvoluted peaks centered at 286.3 and 289.3 eV verified the presence of C–O and C = O bonds, respectively [28]. Interestingly, in the CuO/cGQDs nanohybrid, the distinct peaks of C 1 s presented an apparent shift to lower binding energy, demonstrating decrease of electron density according to previous literature [29]. In such process, electrons were shuttled smoothly and rapidly from cGQDs to CuO through the interface and thus the whole electrocatalytic activity of CuO were accelerated. All above results demonstrated the successful formation of CuO/cGQDs heterostructure with a strong interaction and the inner theoretical elucidation of the improved redox and electron transfer capability.

Electrochemical behavior investigation

Initially, electrochemical performance of the CuO/cGQDs nanocomposite was explored by cyclic voltammograms (CVs). As depicted in Fig. 3A, the CuO/cGQDs decorated electrodes attained higher current response compared with electrodes modified by pristine CuO or cGQDs even in the PBS. After injection of DA, higher current and apparent redox peaks were spotted in CV curves of all electrodes, especially CuO and CuO/cGQDs decorated electrodes owing to good redox capability of CuO. Moreover, electrodes coated with CuO/cGQDs nanocomposite obtained the highest oxidative and reductive current due to superior electron mobility of cGQDs. Taking this into account, CS/CuO/cGQDs/GCE was applied as working electrodes for subsequent measurements to evaluate the electrocatalytic property of nanohybrid. Subsequently, optimization for the sensing performance was implemented by modulating the concentration ratio of CuO and cGQDs (Fig. 3B). When one portion of cGQDs attached on four portions of CuO, the peak current reached the maximum, indicating that the biosensor attained optimum synergistic effect towards DA

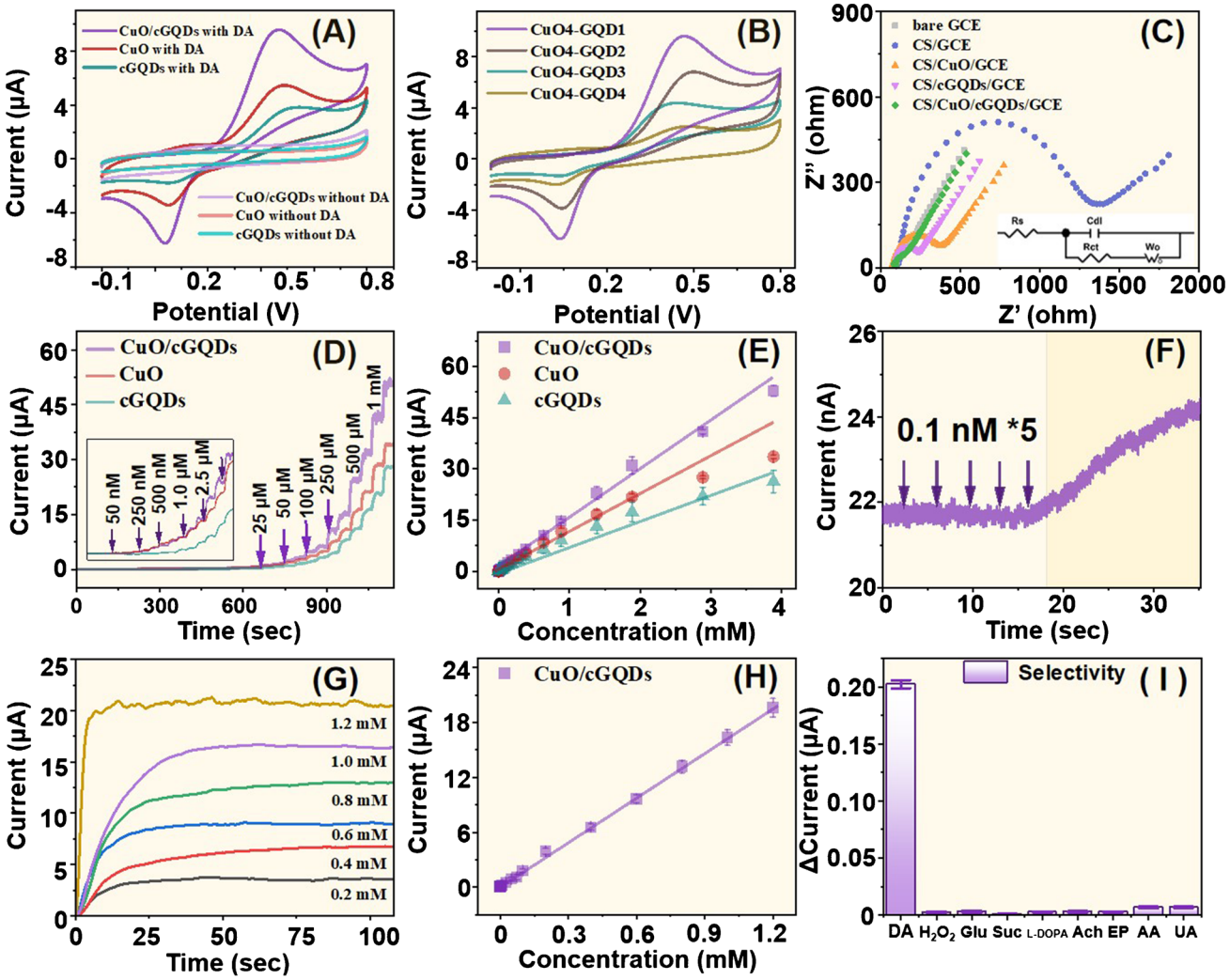

Fig. 3 Electrocatalytic characters of the decorated electrodes: (**A**) CV curves of various electrodes with and without DA, respectively (bare CuO, bare cGQDs and CuO/cGQDs coated GCE). (**B**) CV curves of electrodes with different CuO/cGQDs ratios. CV tests were operated in 0.01 M PBS containing 0.5 mM DA. (**C**) EIS curves of various electrodes (bare GCE, CS coated, CuO coated, cGQDs coated, and CuO/cGQDs coated GCE) in 5 mM $[Fe(CN)_6]^{-3/-4}$ (1:1) + 0.1 M KCl; (**D**) Amperometric response towards increasing DA concentration for bare CuO, bare cGQDs and CuO/cGQDs coated GCE; (**E**) Calibration plots for exact current versus increasing DA concentrations according to (**D**); (**F**) LOD investigation by amperometric response towards subsequent additions of 0.1 nM DA for CS/CuO/cGQDs/GCE; (**G**) Amperometric response towards different concentrations of DA for CS/CuO/cGQDs/GCE; (**H**) Calibration plots for exact current versus increasing DA concentrations according to (**G**); (**I**) Selectivity investigation by amperometric response of CS/CuO/cGQDs/GCE towards 0.01 mM DA along with 0.1 mM interfering elements, all amperometric response were tested in 0.01 M PBS at + 0.45 V vs. Ag/AgCl

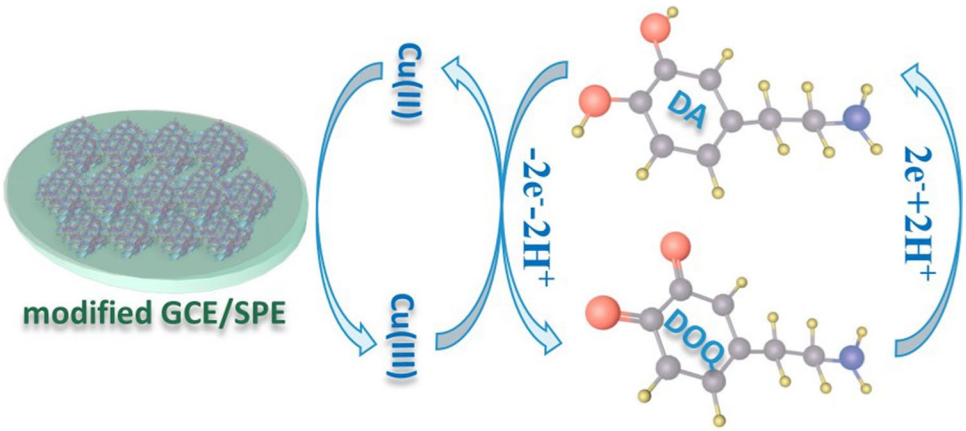

Scheme 2 The electrooxidation mechanism: DA was oxidized to DOQ by Cu(III), who turned to Cu(II)

oxidation. The result elucidated the dominant role of CuO in the process of DA oxidation. Moreover, higher portions of CuO in such system promoted the electrocatalytic activity via higher affinity and recognition capabilities, which was in consistence with previous literature [30]. Meanwhile, as an auxiliary role, cGQDs could improve interfacial reaction rate through π–π stacking interactions between DA and cGQDs as well as accelerated electron mobility, lubricating the electrochemical sensing for DA determination [12]. However, overdense packing of cGQDs may in turn increase the resistance of charge transfer and consequently hamper the interactions between sensing material and the target molecules. As a result, CuO and cGQDs at the mass ratio of 4:1 was deemed as the best ratio and applied in the further electrochemical research towards DA determination. Figure S3A presented the CV curves of the sensor towards detection of DA at various concentrations. As the concentration of DA increased from 200 to 500 μM, the oxidation peak current enhanced gradually and a well-defined anode peak was situated roughly at + 0.45 V vs. Ag/AgCl. The results indicated that CuO/cGQDs nanohybrid was a suitable candidate for the sensitive determination of DA.

According to a previous study [31], it could be extrapolated that two electrons and protons were produced and flowed towards the conduction area of the sensor base during the electrochemical oxidation of DA. Therefore, the fabricated electrodes obtained enhanced anodic peak current, as illustrated in Scheme 2.

Briefly, conversion from DA to dopamine-o-quinone (DOQ) was in accordance with valence change of Cu (from Cu(III) to Cu(II)). Moreover, owing to the following reasons, greatly electroactive process occurred on the interface of the CuO/cGQDs modified electrode. First, CuO presented favorable electrochemical redox capability for catalytic activity; meanwhile, the continuous 3DIO structure provided vast surface area, which lubricated the diffusion of target analyte and thus fully interacted with sensitive materials. Second, the analysis for the XPS spectra of O 1 s confirmed that the CuO/cGQDs nanocomposite attained more deficient oxygen on the interface, which enhanced electron mediator-oxygen vacancies. In this way, the accelerated charge transfer led to improving electrocatalytic capability and therefore obtained improved electrochemical sensing performance [27]. Third, besides fast shuttling capability, the cGQDs endowed the nanocomposite with high affinity and recognizing capability owing to the π–π stacking interactions between DA and graphene as well as connection between carboxyl form cGQDs and amino from DA [12]. Ultimately, integration of CuO and cGQDs produced numerous heterojunctions at the interface, which performed as catalytically active layer and electron transport booster to yield robust and smooth oxidation for DA towards DOQ. As a result, accurate and ultrasensitive determination of DA was achieved with promising potential for biological application.

CV experiments at different scan rates were implemented to explore the inner kinetics of the electrochemical oxidation of DA on the surface of the CuO/cGQDs/GCE. As the Figure S3B demonstrated, with the scan rate increasing, gradually increased oxidation peak current was spotted and the oxidative peak potential centered away from 0.45 V vs. Ag/AgCl further. Moreover, as presented in the Figure S3C, the current density of oxidation and reduction peak was directly proportional to square root of scan rate with the correlation coefficients (R^2) value of 0.9900 and 0.9986 for the relationship, which indicated that diffusion mechanism suited perfectly for the DA oxidation during the electrochemical sensing process. Such controlled approach contributed to accelerated electron transfer activity, which was conducive to the electrochemical determination of DA.

Subsequently, the electrochemical impedance spectroscopy (EIS) technique worked as clear illustration for interface characteristics of various electrodes. The Nyquist plots of various materials modified GCE in surrounding containing $[Fe(CN)_6]^{3-/4-}$ were presented in Fig. 3C. The Nyquist plot was composed only of a straight line and semi-circle

in the low and high frequencies domain, respectively. The straight line indicated fast charge-transfer kinetics and slower mass transfer. The higher frequencies semicircle diameter correlated closely to electron transfer limitation (R_{ct}), which depended on charge-transfer resistance. Moreover, to determine the actual R_{ct} value for every plots, a simple equivalent circuit was applied as measurement model in the inset of Fig. 3C. The solution resistance (R_s), charge transfer resistance (R_{ct}), and double layer capacitance (C_{dl}) were clearly revealed in such circuitry. An obviously linear plot was attained using bare GCE (63.8 Ω) due to brilliant electrical conductivity. After coated with CS, the diameter of the semicircular plot increased obviously (1.1 kΩ) owing to high electron-transfer resistance of CS. Furthermore, the R_{ct} values decreased as following: CuO/GCE (262.3 Ω), cGQDs/GCE (150.4 Ω), and CuO/cGQDs/GCE (83.5 Ω), indicating that CuO/cGQDs nanocomposite may exhibit superior electrochemical performance for vast electrode surface area along with accelerated charge transport.

Amperometric measurements were further operated to investigate the catalytic performance of CuO/cGQDs modified electrodes. To begin with, the working potential was set as 0.45 V vs. Ag/AgCl since the oxidative current reached anode peak at 0.45 V vs. Ag/AgCl in CV curve of the prepared CuO/cGQDs/GCE (purple curve in Fig. 3A). Therefore, the chronoamperometry tests for modified electrodes were implemented in PBS containing increasing DA amount at + 0.45 V vs. Ag/AgCl (Fig. 3D). The correlated calibration plots were illustrated in Fig. 3E and the related data were calculated and summarized in Table S1, which exhibited essential sensing parameters (sensitivity, linear range and so on) of the current electrodes. According to curves and table above, it was intuitional and reasonable to make comparison of sensing performance for pristine CuO, pristine cGQDs, and CuO/cGQDs nanocomposite. The amperometric response of bare GCE and its calibration plot were also recorded as presented in Figure S4A&B, which convinced that the nanocomposite coated one attained better sensing performance. In consistence with the result in CVs (Fig. 3A), CuO/cGQDs nanocomposite attained enhanced monitoring effect compared to pristine CuO and cGQDs, owing that the heterostructure presented good synergistic capability for recognizing and shuttling activity. Moreover, according to Fig. 3E, the CuO/cGQDs modified sensor showed excellent sensitivity of 243.45 μA mM^{-1} cm^{-2} along with the theoretical detection limit of 6.9 nM (signal-to-noise ratio (S/N) = 3) in the broad linear range of 0.05–1888.5 μM. Specifically, a practical low LOD of 0.5 nM was attained by amperometric measurement, as visualized in Fig. 3F , indicating the excellent electrocatalytic ability of the prepared sensor. To continue, the modified electrodes possessed excellent precision owing that addition of same amount DA in another way made no significant difference in linear range and sensitivity (Fig. 3G, H and Figure S4C, D). Meanwhile, several previous typical DA biosensors were outlined to evaluate the exact monitoring performance of the CuO/cGQDs modified electrode in this work. As shown in Fig. 4 and Table S2, the supposed biosensor was prominent for its good sensitivity, comparable linearity range, and a relatively lower LOD [6, 32–38], which indicated the excellent electrocatalytic activity towards DA along with enhanced electrical conductivity of such heterostructure. Furthermore, this investigation definitely lay solid foundation for its promising implementation in real-time DA determination, especially for neurological diseases with abnormal DA fluctuation.

Specificity, repeatability and stability were necessary parameters for implementing the DA sensor during biomedical studies. The selectivity of the prepared sensor was evaluated by amperometry test operated in PBS with the successive additions of DA and some commonly coexisted interferences such as hydrogen peroxide (H_2O_2), glucose (Glu), sucrose (Suc), L-DOPA, acetylcholine (Ach), epinephrine (EP), AA, and UA. As Fig. 3I suggested, the sensor possessed good specificity as DA obtained a significant current response compared with other biological compounds at the implemented potential. It might be elucidated that the negatively charged (the zeta potential was approximately − 10.47 mV) CuO/cGQDs tended to interact with positively charged DA through electrostatic attraction rather than negatively charged AA and UA which may cause negative repulsion. Moreover, the cGQDs may account a lot for recognition of DA via interaction between carboxyl from cGQDs and amino from DA, which also explained the better affinity to DA than other neurotransmitters such as L-DOPA, Ach, and EP. Next, the repeatability test was operated by applying a single CuO/cGQDs modified electrode for five

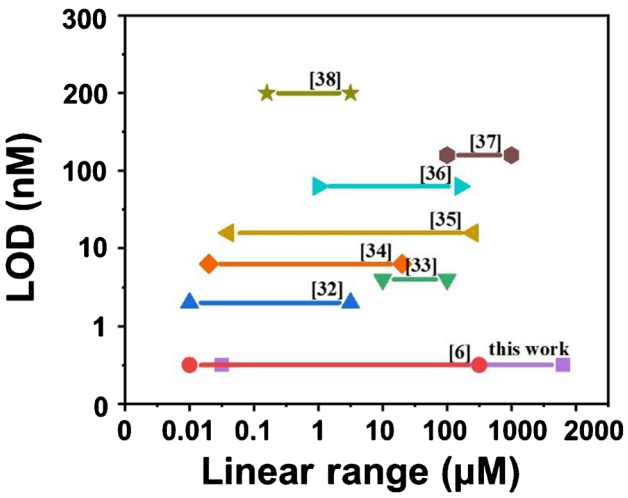

Fig. 4 Sensing performance comparison for the fabricated sensor: the LOD and linear range of previous electrochemical DA sensors comparing with the CuO/cGQDs based sensor

times to monitor 100 μM of DA in PBS solution (0.01 M) and attained relative standard deviation (RSD) of 0.84% (Figure S5A). The same operation was implemented on five electrodes to evaluate the reproducibility, which gained RSD of 1.04% (Figure S5B). Note that there was no presence of carryover effects on account that the sensor performed nearly instantaneous response to changing DA concentration and maintained activity after several operational times (Figure S5C). As for reversibility evaluation, the electrode was put in 100 μM and 5 μM DA solutions alternately (each internal was 30 min), during which the current response displayed reversible changes even after five cycles (Figure S5D). Eventually, the operational stability was evaluated by attaining the continuous current response to 100 μM DA for 10 h, indicating an average variation of 10% as the Figure S6A presented. Furthermore, the response to 100 μM of DA (5 weeks) was constantly recorded to assess the storage stability of the prepared sensor. The CuO/cGQDs modified electrodes attained an RSD of 1.08% and the current response maintained as high as 97.2% level after 5 weeks (Figure S6B). All characteristic sensing capacity investigations above confirmed that such electrochemical biosensor suited perfectly to detection of DA in biological samples.

Feasibility investigation

The sensing operation at biofluid and cellular level was conducted to confirm the practicability for DA determination. Initially, feasibility for DA detection was tested in a more complicated surrounding like artificial blood, FBS, and artificial urine. In such particular environment including diverse proteins and ions, it was a challenge for the biosensor to monitor DA accurately. Before measurement, dilution was implemented for the artificial biofluid and subsequently it was spiked with three different concentrations of DA. Interestingly, the sensor conducted brilliant response to different amount of DA, which matched well with the actual addition with the recovery of 100.1–101.6%, 99.8–102.0%, and 99.6–101.3% for artificial blood, FBS, and artificial urine respectively (Table S3-S5). These explorations demonstrated the promising clinical feasibility of the CuO/cGQDs modified sensor for detecting DA at abnormal level in biological fluids, particularly in blood and urine. Furthermore, such anti-interference capability provided promising feasibility for conversion to point-of-care treatment (POCT) platform, which was prominent in future medical research and application.

Recognizing fluctuation of DA at cellular level was imperative on account that abnormal DA level was allied with occurrence of several neurological diseases like Parkinson's disease and euphoria. Moreover, according to previous record, potassium ions (K^+) fluctuation in the central nervous system would lead to secretion of DA, contributing to neurological disorders [39]. Therefore, for the exquisite illustration of dopaminergic neurotransmission, it was reasonable to track the K^+-induced DA efflux of neural cells such as PC12 cells. As shown in Fig. 5A, as the extracellular K^+ levels increased, the cell membrane would depolarize and Ca^{2+} channels would open, which in turn elevated the intracellular Ca^{2+} level and therefore evoked the efflux of DA [40]. Moreover, calcium channel antagonist (CdI_2) was applied to pretreat the PC12 cells to confirm the significant role of Ca^{2+} channel during K^+-stimulated secretion of DA. As shown in Fig. 5B, the voltage-dependent calcium channels (VDCC, a special transporting channel modulated by change of membrane potential) were blocked by CdI_2 and therefore the conduction and exocytosis of DA was impeded. The real-time measurement was implemented in PBS under gently stirring. As demonstrated in Fig. 5D, no fathomable signal was attained from PC12 cells without inducement of K^+ at the working potential. After K^+ was injected continuously, amperometric current significantly increased, indicating the exocytosis of DA from PC12 cells. Furthermore, the little decrement in current response after initial two injections of K^+ might be elucidated by decreased DA vesicle. Ultimately, with K^+ inducement after CdI_2 pretreatment, the cells generated nearly no obvious current signal, verifying the involvement of Ca^{2+} channel for DA efflux after the K^+ inducement.

On account that the abnormal levels of DA in neural cells were correlated with neurological diseases, dopaminergic drugs had been emphasized as optimum therapeutic methods. As for schizophrenia, the dominant treatment was performed by antipsychotic drugs, which modulated dopaminergic functions by impeding DA receptor activities and thus limiting K^+-evoked DA secretion. As shown in Fig. 5C, haloperidol (D2 receptors antagonist), once it binded to D2 receptor (D2R) on a plasma membrane, the conduction of DA and exocytosis of DA were hampered [41]. In this regard, haloperidol (0–10 μM) were initially incubated with PC12 cells and K^+ (50 mM) was applied subsequently. As displayed in Fig. 5E, the level of DA release decreased with the increasing amount of haloperidol, indicating that antipsychotic drugs may inhibit intracellular DA secretion from PC12 cells. The results convinced that haloperidol was able to affect the intracellular DA level, which was in consistence with the previous report [42]. Therefore, the sensor successfully evaluated the efficacy of antipsychotic drugs upon DA secretion, which could provide brilliant assessing protocol for management of DA-related diseases.

Subsequently, the biocompatibility of CuO/cGQDs nanocomposite was explored by culturing PC12 cells with media containing the nanohybrid. As presented in Figure S7, there was no significant changes in microscopic structure after pretreatment with CuO/cGQDs. Moreover, CCK-8 assay was subsequently implemented to verify the cytotoxicity of

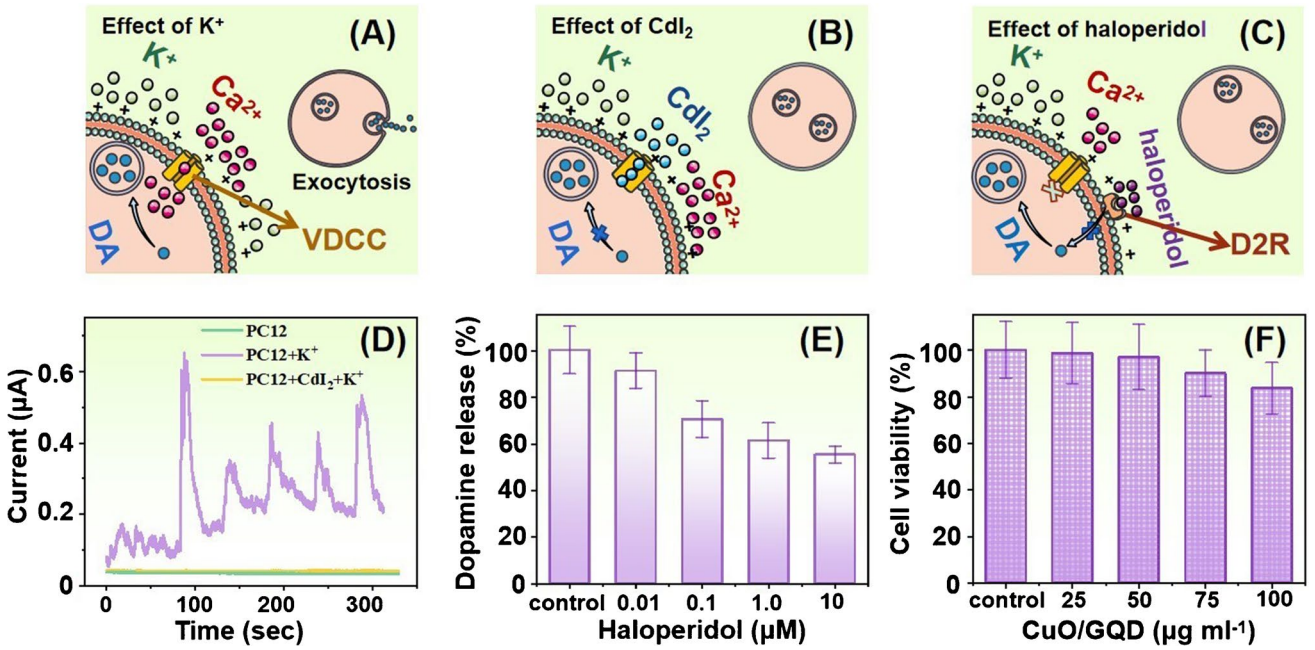

Fig. 5 Feasibility investigation for neural cell using the modified electrodes. (**A**) Scheme for mechanism of K^+-induced DA secretion from PC12 cell (open Ca^{2+} channels). (**B**) Scheme for the mechanism of CdI_2-hampered DA secretion of PC12 cell (block VDCC and then impede DA exocytosis). (**C**) Scheme for the mechanism of haloperidol-influenced DA secretion of PC12 cell (bind to D2R and impede DA exocytosis). (**D**) Efficacy investigation of K^+ and CdI_2 for DA efflux of PC12 cells in 0.01 M PBS. The control group was not pretreated with K^+ and CdI_2. (**E**) Efficacy investigation of haloperidol for DA efflux of PC12 cells. The control group was not pretreated with haloperidol. (**F**) Biocompatibility investigation of CuO/cGQDs nanocomposite: cell viability was measured for PC12 cells pretreated with and without CuO/cGQDs

the nanohybrid. Figure 5F demonstrated the survival rate after CuO/cGQDs were added to culture solution of PC12 cells for 24 h. With CuO/cGQDs concentration increased (0.025–0.1 mg mL^{-1}), cells viability was decreased from 98.5 to 85.3%. These results confirmed the good biocompatibility of the nanosystem of CuO/cGQDs and the promising practicability of the supposed biosensor for DA detection at a cellular level. Moreover, this indicated the possibility to apply such nanocomposite for in situ sensing of DA with little cell toxicity.

The occurrence of PD and its treatment were in consistency with DA fluctuation. Thus, animal models of PD were used to understand dopaminergic neurotransmission of PD and investigate the monitoring feasibility of such DA biosensor. Reserpine was utilized to construct PD model owing to its inhibitory effect on vesicular monoamine transporter, which consequently causes decreased vesicular DA stores in the striatum [43]. Afterwards, co-administration of L-DOPA and benserazide was implemented to alleviate the symptoms of PD (including akinesia, rigidity, etc.) temporarily. Figure 6A clearly plotted the whole process of animal study and Figure S8 presented the image for CSF collection from the citerna magna using micropipette. In this experiment, after injection of reserpine, the mice demonstrated characteristic behavioral state such as tremor and bradykinesia, which was not spotted in the normal group. However, such symptoms disappeared when the mice were treated with L-DOPA and benserazide. Then the changing DA level in plasma and CSF was monitored by CuO/cGQDs modified SPE instead of GCE owing to low volume testing fluid. In this regard, the sensing performance of CuO/cGQDs modified SPE was first investigated in PBS, as Figure S9 illustrated, the CV plot verified that the supposed composite possessed brilliant redox capability and the oxidative peak situated at 0.35 V, which was chosen as the working potential for following chronoamperometry tests. Figure S10 exhibited chronoamperograms along with correlated calibration plots for the exactly modified electrode with the excellent sensitivity of 7450 (0.1–1 nM) and 390 (1–500 nM) μA mM^{-1}. On this basis, the variation of DA level in the prepared plasma sample was spotted as shown in Fig. 6B, the reserpine inducement led to a clear decrease and L-DOPA/benserazide treatment latter contributed to an increment in the current signal, respectively. The similar condition happened to investigation of CSF samples except a little higher current response for all groups (Fig. 6C). The current intensity difference of plasma and CSF might be assigned to the exact physiological function of CSF in nervous systems, which enabled the enrichment of neurotransmitter such as DA. Hence, this sensor could spot DA fluctuation in biofluid such as plasma and

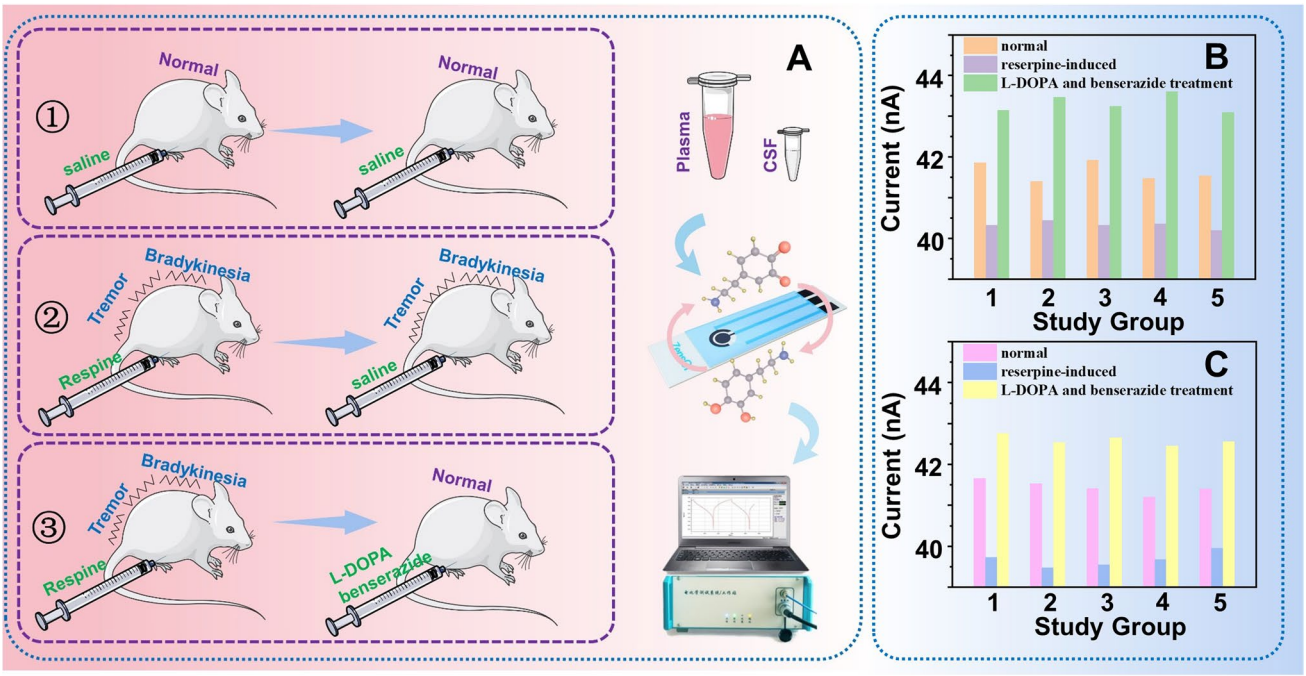

Fig. 6 Feasibility investigation for animal model using the modified electrodes: (**A**) Scheme for animal study model of PD: ① the normal group, ② the only reserpine induced group, ③ the reserpine induced group following with treatment of L-DOPA and benserazide. The blood and CSF of each group were collected for electrochemical measurement. (**B**) Amperometric response of DA in CSF of the control, only reserpine-induced, and reserpine followed by L-DOPA-treated mice. (**C**) Amperometric response of DA in plasma of the control, only reserpine-induced, and reserpine followed by L-DOPA-treated mice

CSF, showing brilliant potential in recognition and long-term monitor of DA-related diseases.

Conclusion

In this work, a facile homogeneous CuO/cGQDs based electrochemical biosensor was developed for DA determination in artificial biofluid, stimulated neural cells and even real pathological sample from animal model. The adopted 3DIO structure with continuous microstructure provided vast surface area; meanwhile, the QDs with superior conductivity accelerated the electron transfer. As a result, the target analyte diffused rapidly and contacted with the sensing materials easily, contributing to brilliant electrocatalytic capability and splendid detecting performance. The prepared biosensor could distinguish DA in neutral environment containing as low concentration as 0.05 nM DA and in existence of interferences (AA, UA, H_2O_2, Glu, and Suc), demonstrating excellent sensitivity and selectivity of our method. The obtained sensor successfully achieved detection of DA from complex matrix such as artificial blood, FBS, and artificial urine, avoiding troublesome sample preparation as other sensing method. Moreover, it also did well in real-time and in-situ determination DA efflux from PC12 upon K^+ stimulation, which provided smart strategy for diagnosis of DA-related neurological disorders. In this regard, we further investigated the efficacy of antipsychotic drugs using the prepared sensor and found that the expression of intracellular DA dropped as the drug concentration increased. In this way, the biosensor could be implemented as evaluation tool for management of psychiatric diseases. Ultimately, as an intuitional tool to learn about symptomatology and neuropathology of DA-related diseases, animal model of PD was constructed to investigate the feasibility for the biosensor to monitor DA fluctuation in plasma and CSF. All in all, this study put forward insightful protocol for the physiological and pathological study as well as clinical diagnosis and treatment correlated to various neurological and psychiatric diseases.

Supplementary Information The online version contains supplementary material available at https://doi.org/10.1007/s00604-022-05479-z.

Funding This work was supported by the National Science Foundation of China (82170998 and 61874049), General program of Natural Science Foundation of Jilin Province (20200201356JC, 20200201317JC, 20180101210JC and 20200801017GH), seed grant from Jilin University School of Dentistry, and the Fundamental Research Funds for the Central Universities.

Declarations

Competing interests The authors declare no competing interests.

References

1. Wise A. Roy (2004). Dopamine, learning and motivation Natural Reviews Neuroscience.5:483–94.
2. Nagy J, Lee T, Seeman P, Fibiger H (1978) Direct evidence for presynaptic and postsynaptic dopamine receptors in brain. Nature 274:278–281
3. Noroozifar M, Khorasani-Motlagh M, Akbari R, Parizi MB (2011) Simultaneous and sensitive determination of a quaternary mixture of AA, DA, UA and Trp using a modified GCE by iron ion-doped natrolite zeolite-multiwall carbon nanotube. Biosens Bioelectron 28(1):56–63
4. Pham Ba VA, Cho D-g, Hong S (2019) Nafion-radical hybrid films on carbon nanotube transistors for monitoring antipsychotic drug effects on stimulated dopamine release. ACS Appl Mater Interfaces 11:9716–9723
5. Oh J, Lee JS, Jun J, Kim SG, Jang J (2017) Ultrasensitive and selective organic FET-type nonenzymatic dopamine sensor based on platinum nanoparticles-decorated reduced graphene oxide. ACS Appl Mater Interfaces 9:39526–39533
6. Senel M, Dervisevic M, Alhassen S, Alachkar A, Voelcker NH (2020) Electrochemical micropyramid array-based sensor for in situ monitoring of dopamine released from neuroblastoma cells. Anal Chem 92:7746–7753
7. Alachkar A, Alhassan S, Senel M (2022) Lab-in-a-syringe: a novel electrochemical biosensor for on-site and real-time monitoring of dopamine in freely behaving mice. ACS sensors 331–37
8. Senel M, Dervisevic E, Alhassen S, Dervisevic M, Alachkar A, Cadarso VJ et al (2020) Microfluidic electrochemical sensor for cerebrospinal fluid and blood dopamine detection in a mouse model of parkinson's disease. Anal Chem 92:12347–12355
9. Zhang X, Zhang CJ, Abas A, Zhang Y, Mu X, Zhou J et al (2019) Ag nanoparticles enhanced vertically-aligned CuO nanowire arrays grown on Cu foam for stable hybrid supercapacitors with high energy density. Electrochim Acta 296:535–544
10. Yang S, Sun J, Xu L, Zhou Q, Chen X, Zhu S et al (2020) Au@ ZnO functionalized three–dimensional macroporous WO3: a application of selective H2S gas sensor for exhaled breath biomarker detection. Sensors Actuators B Chem 324:128725
11. Ahmadi N, Bagherzadeh M, Nemati A (2020) Comparison between electrochemical and photoelectrochemical detection of dopamine based on titania-ceria-graphene quantum dots nanocomposite. Biosens Bioelectron 151:111977
12. Jackowska K, Krysinski P (2013) New trends in the electrochemical sensing of dopamine. Anal Bioanal Chem 405:3753–3771
13. Hashemzadeh N, Hasanzadeh M, Shadjou N, Eivazi-Ziaei J, Khoubnasabjafari M, Jouyban A (2016) Graphene quantum dot modified glassy carbon electrode for the determination of doxorubicin hydrochloride in human plasma. J Pharm Anal 6:235–241
14. Ben Aoun S (2017) Nanostructured carbon electrode modified with N-doped graphene quantum dots–chitosan nanocomposite: a sensitive electrochemical dopamine sensor. Roy Soc Open Sci 4:171199
15. Huang Q, Lin X, Tong L, Tong Q-X (2020) Graphene quantum dots/multiwalled carbon nanotubes composite-based electrochemical sensor for detecting dopamine release from living cells. ACS ACS Sustain Chem Eng 8:1644–1650
16. Imani R, Emami SH, Faghihi S (2015) Nano-graphene oxide carboxylation for efficient bioconjugation applications: a quantitative optimization approach. J Nanopart Res 17:1–15
17. Kim J, Jang W, Kim JH, Yang C-M (2021) Synthesis of graphene quantum dots-coated hierarchical CuO microspheres composite for use as binder-free anode for lithium-ion batteries. Compos Part B-Eng 222:109083
18. Geim A, Novoselov K (2007) Nature Mater 6:183
19. Zhu J, Zeng G, Nie F, Xu X, Chen S, Han Q et al (2010) Decorating graphene oxide with CuO nanoparticles in a water–isopropanol system. Nanoscale 2:988–994
20. Amara U, Riaz S, Mahmood K, Akhtar N, Nasir M, Hayat A et al (2021) Copper oxide integrated perylene diimide self-assembled graphitic pencil for robust non-enzymatic dopamine detection. RSC Adv 11:25084–25095
21. Anandan S, Yoon M (2003) Photocatalytic activities of the nanosized TiO2-supported Y-zeolites. J Photoch Photobio C 4:5–18
22. Prajapati AK, Mondal MK (2021) Development of CTAB modified ternary phase α-Fe2O3-Mn2O3-Mn3O4 nanocomposite as innovative super-adsorbent for Congo red dye adsorption. J Environ Chem Eng 9:104827
23. Reddy S, Swamy BK, Jayadevappa H (2012) CuO nanoparticle sensor for the electrochemical determination of dopamine. Electrochim Acta 61:78–86
24. Huang S, Song L, Xiao Z, Hu Y, Peng M, Li J et al (2016) Graphene quantum dot-decorated mesoporous silica nanoparticles for high aspirin loading capacity and its pH-triggered release. Anal Methods 8:2561–2567
25. Wu X, Zhang Y, Han T, Wu H, Guo S, Zhang J (2014) Composite of graphene quantum dots and Fe_3O_4 nanoparticles: peroxidase activity and application in phenolic compound removal. SC Adv 4:3299–3305
26. Zhou X, Xu L, Lv J, Yang S, Zhu S, Chen X et al (2019) Au anchored three-dimensional macroporous NiO@ CuO inverse opals for in-situ sensing of hydrogen peroxide secretion from living cells. Sensors Actuators B Chem 297:126729
27. Zhao W, Wang W, Shi H (2020) 2D/2D Z-scheme BiO1-XBr/g-C3N4 heterojunction with rich oxygen vacancies as electron mediator for enhanced visible-light degradation activity. Appl Surf Sci 528:146925
28. Dinh LN, Ramana LN, Agarwal V, Zetterlund PB (2020) Miniemulsion polymerization of styrene using carboxylated graphene quantum dots as surfactant. Polym Chem 11:3217–3224
29. Zhu M, Kim S, Mao L, Fujitsuka M, Zhang J, Wang X et al (2017) Metal-free photocatalyst for H2 evolution in visible to near-infrared region: black phosphorus/graphitic carbon nitride. J Am Chem Soc 139:13234–13242
30. Daemi S, Ghasemi S, Ashkarran AA (2019) Electrospun CuO-ZnO nanohybrid: tuning the nanostructure for improved amperometric detection of hydrogen peroxide as a non-enzymatic sensor. J Colloid Interf Sci 550:180–189
31. Chen T-W, Chinnapaiyan S, Chen S-M, Ali MA, Elshikh MS, Mahmoud AH (2020) A feasible sonochemical approach to synthesize CuO@ CeO2 nanomaterial and their enhanced non-enzymatic sensor performance towards neurotransmitter. Ultrason Sonochem 63:104903
32. Emran MY, Shenashen MA, Morita H, El-Safty SA (2018) One-step selective screening of bioactive molecules in living cells using sulfur-doped microporous carbon. Biosens Bioelectron 109:237–245
33. Paramparambath S, Shafath S, Maurya MR, Cabibihan J-J, Al-Ali A, Malik RA et al (2021) Nonenzymatic electrochemical sensor based on CuO-MgO composite for dopamine detection. IEEE Sens J 21:25597–25605
34. Li B, Zhou Y, Wu W, Liu M, Mei S, Zhou Y et al (2015) Highly selective and sensitive determination of dopamine by the novel

molecularly imprinted poly (nicotinamide)/CuO nanoparticles modified electrode. Biosens Bioelectron 67:121–128
35. Xie X, Wang DP, Guo C, Liu Y, Rao Q, Lou F et al (2021) Single-atom ruthenium biomimetic enzyme for simultaneous electrochemical detection of dopamine and uric acid. Anal Chem 93:4916–4923
36. Zhang W, Jia G, Li Z, Yuan C, Bai Y, Fu D (2017) Selective electrochemical detection of dopamine on polyoxometalate-based metal–organic framework and its composite with reduced graphene oxide. Adv Mater Interfaces 4:1601241
37. Saraf M, Natarajan K, Saini AK, Mobin SM (2017) Small biomolecule sensors based on an innovative MoS 2–rGO heterostructure modified electrode platform: a binder-free approach. Dalton T 46:15848–15858
38. Abdelbasir S, El-Sheikh S, Morgan V, Schmidt H, Casso-Hartmann L, Vanegas D et al (2018) Graphene-anchored cuprous oxide nanoparticles from waste electric cables for electrochemical sensing. ACS Sustain Chem Eng 6:12176–12186
39. Kofuji P, Newman E (2004) Potassium buffering in the central nervous system. Neuroscience 129:1043–1054
40. Miao Y-L, Stein P, Jefferson WN, Padilla-Banks E, Williams CJ (2012) Calcium influx-mediated signaling is required for complete mouse egg activation. Proc Natl Acad Sci 109:4169–4174
41. Matsuo T, Izumi Y, Wakita S, Kume T, Takada-Takatori Y, Sawada H et al (2010) Haloperidol, spiperone, pimozide and aripiprazole reduce intracellular dopamine content in PC12 cells and rat mesencephalic cultures: implication of inhibition of vesicular transport. Eur J Parm 640:68–74
42. Tyler MW, Yourish HB, Ionescu DF, Haggarty SJ (2017) Classics in chemical neuroscience: ketamine. ACS Chem Neurosci 8:1122–1134
43. Leão AH, Sarmento-Silva AJ, Santos JR, Ribeiro AM, Silva RH (2015) Molecular, neurochemical, and behavioral hallmarks of reserpine as a model for Parkinson's disease: new perspectives to a long-standing model. Brain Pathol 25:377–390